Temperature–Salinity Structure of the North Atlantic Circulation and Associated Heat and Freshwater Transports

XIAOBIAO XU

Center for Ocean–Atmospheric Prediction Studies, Florida State University, Tallahassee, Florida

PETER B. RHINES

University of Washington, Seattle, Washington

ERIC P. CHASSIGNET

Center for Ocean–Atmospheric Prediction Studies, Florida State University, Tallahassee, Florida

ABSTRACT

This study investigates the circulation structure and relative contribution of circulation components to the time-mean meridional heat and freshwater transports in the North Atlantic, using numerical results of a high-resolution ocean model that are shown to be in excellent agreement with the observations. The North Atlantic circulation can be separated into the large-scale Atlantic meridional overturning circulation (AMOC) that is diapycnal and the subtropical and subpolar gyres that largely flow along isopycnal surfaces but also include prominent gyre-scale diapycnal overturning in the Subtropical Mode Water and Labrador Sea Water. Integrals of the meridional volume transport as a function of potential temperature θ and salinity S yield streamfunctions with respect to θ and to S, and heat functions. These argue for a significant contribution to the heat transport by the southward circulation of North Atlantic Deep Water. At 26.5°N, the isopycnic component of the subtropical gyre is colder and fresher in the northward-flowing western boundary currents than the southward return flows, and it carries heat southward and freshwater northward, opposite of that of the diapycnal component. When combined, the subtropical gyre contributes virtually zero to the heat transport and the AMOC is responsible for all the heat transport across this latitude. The subtropical gyre however significantly contributes to the freshwater transport, reducing the 0.5-Sv (1 Sv ≡ 10^6 m^3 s^{-1}) southward AMOC freshwater transport by 0.13 Sv. In the subpolar North Atlantic near 58°N, the diapycnal component of the circulation, or the transformation of warm saline upper Atlantic water into colder fresher deep waters, is responsible for essentially all of the heat and freshwater transports.

1. Introduction

Large-scale ocean circulations play an important role in the earth's climate by carrying and redistributing heat and freshwater (or salinity anomaly) through ocean basins and by interacting with the atmosphere. The oceanic heat transport has been shown to be instrumental in warming the global mean climate (Herweijer et al. 2005), maintaining a warmer Northern Hemisphere (Kang et al. 2015), positioning the intertropical convergence zone and associated rainfall (Kang et al. 2008), feeding the wintertime atmosphere's zonal asymmetry (Rhines et al. 2008), controlling high-latitude decadal warming events (Msadek et al. 2014), and modulating abrupt reductions in the Arctic sea ice under increased greenhouse emission conditions (Holland et al. 2006). The oceanic freshwater transport influences the global atmospheric latent heat transport through ocean–atmosphere moisture exchanges and balances the atmospheric water vapor transport (Bryden and Imawaki 2001).

The North Atlantic heat transport is maximum near 25°N in the subtropics ($\sim$1.3 $\times$ 10^{15} W or 1.3 PW; e.g., Hall and Bryden 1982; Johns et al. 2011; Macdonald and Baringer 2013), where it contributes about one-quarter

of the total ocean–atmosphere heat transport (e.g., Wunsch 2005). This ocean heat transport is traditionally decomposed into the vertical "overturning" and horizontal "gyre" components, computed from multiplication of the zonally averaged (along constant depth) velocity and temperature profiles and multiplication of the deviations from the zonal averages, respectively (e.g., Bryden and Imawaki 2001). This decomposition usually results in the vertical component being responsible for ~90% of the northward heat transport at 25°N and the horizontal component being responsible for the remaining ~10% (e.g., Johns et al. 2011; McCarthy et al. 2015). The vertical component is generally deemed to be the Atlantic meridional overturning circulation (AMOC), while the horizontal component is attributed to the (wind driven) subtropical gyre. The AMOC is a basin-scale circulation pattern in which warm saline water from the South Atlantic is carried northward in the upper limb (approximately above 1000 m), transformed into the colder fresher North Atlantic Deep Water (NADW) in the subpolar North Atlantic as well as in the Nordic seas, and returned southward in the lower limb (1000–4000 m). In contrast, the subtropical gyre is a subbasin-scale pattern in which the water circulates anticyclonically around the subtropical North Atlantic above σ_θ of 27.3–27.4 kg m^{-3} and does not involve deep-water formation.

Msadek et al. (2013) examined in detail the relationship between the ocean heat transport and the AMOC in two widely used climate models, the GFDL Climate Model, version 2.1 (CM2.1), and the NCAR Community Climate System Model, version 4 (CCSM4). They showed that both models underestimate the time-mean heat transport at 26.5°N despite a stronger-than-observed mean AMOC magnitude. This is mainly due to an overly diffusive thermocline in the model, highlighting the important climatic role of the temperature field. They also decomposed the circulation into vertical and horizontal components and found that, contrary to the observations, the horizontal component in both models contributes a weak southward heat transport, opposite of the northward heat transport by the vertical component.

However, this vertical–horizontal decomposition does not necessarily guarantee that the two components actually correspond to the AMOC and the subtropical gyre, respectively. The isopycnals associated with the North Atlantic circulation are not horizontal and have a significant slope across the basin; thus, a zonal average along constant depth mixes very different water masses. When Talley (2003) partitioned the heat transports based on hydrographic data into shallow, intermediate, and deep overturning components, she found that, in the Atlantic Ocean, the shallow overturning within the

subtropical gyre is responsible for a heat transport of 0.1–0.4 PW at 25°N. Thus, although water mass transformation of the AMOC still dominates the North Atlantic heat transport, Talley's (2003) analysis implies that the subtropical gyre may play a more significant role (up to 30% of total heat transport) than would be suggested by a simple vertical versus horizontal decomposition. A similar result was obtained by Ferrari and Ferreira (2011) who, using numerical ocean simulations with and without high-latitude convection to turn on and off the modeled AMOC, suggest that 40% of the oceanic heat transport in the subtropical North Atlantic is due to the wind-driven gyre.

The above-mentioned studies show that there are still large uncertainties about the relative contributions of the AMOC and the subtropical gyre to the heat transport. Even less is known about their contributions to the freshwater transport. In this study, we investigate the heat and freshwater contributions in both subtropical and subpolar regions through a detailed examination of the temperature and salinity structure of the North Atlantic circulation in an eddy-resolving model simulation. The paper is structured as follows: the numerical simulation is briefly summarized in section 2. In section 3, we provide a detailed examination of the various projections of the meridional circulation to describe the structure of the North Atlantic circulation and to compare the model results to the observations. In section 4, we focus on the relative contributions to the heat and freshwater transports of the time-mean flow and temporal variability, of the vertical and horizontal, as well as of the diapycnal and isopycnic circulation components. We find that the model is in excellent agreement with the observations and that, at 26.5°N, the subtropical gyre's contribution to the heat transport is near zero when the transport is decomposed into isopycnal and diapycnal components, less than the value based on the traditional vertical–horizontal decomposition or the values derived by Talley (2003). The main difference between this study and that of Talley (2003) is the way the various water masses are attributed to the AMOC and the subtropical gyre, respectively. The subtropical gyre, on the other hand, significantly contributes to the total freshwater transport, reducing the 0.5-Sv (1 Sv ≡ 10^6 m^3 s^{-1}) southward AMOC freshwater transport by 0.13 Sv. Farther north, in the subpolar region, the diapycnal component of the circulation accounts for essentially all the heat and freshwater transports. The results are summarized and discussed in section 5.

2. Numerical simulation

The North Atlantic and equatorial Atlantic model configuration used in this study is part of a suite of
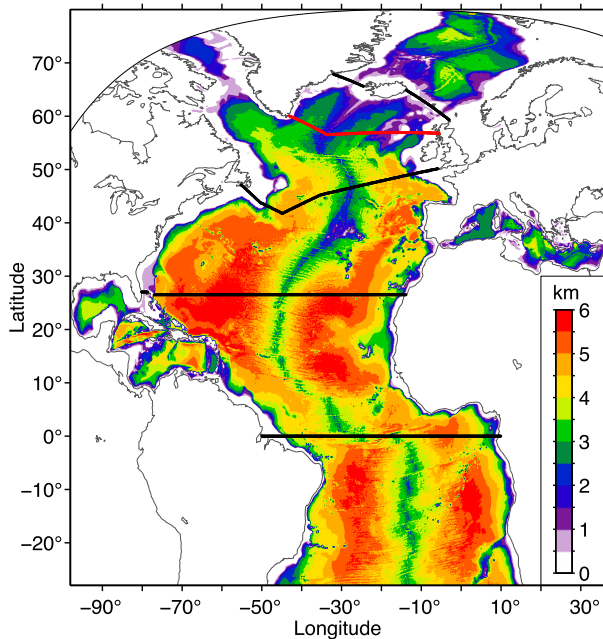
FIG. 1. Model bathymetry along with the location of transatlantic sections. The four black lines from south to north are the equator, 26.5°N, the World Ocean Circulation Experiment (WOCE) section AR19, and the Greenland–Scotland Ridge, respectively. Transports across these sections are displayed in Figs. 4a–d. The red line denotes a section from Cape Farewell to Scotland, across which the results are displayed in Figs. 15–17.

eddy-resolving numerical simulations performed with the Hybrid Coordinate Ocean Model (HYCOM; Bleck 2002; Chassignet et al. 2003) to investigate North Atlantic flow pathways and associated water mass transformations (Xu et al. 2010, 2012, 2013, 2014, 2015). The vertical coordinate of HYCOM is isopycnic in the stratified open ocean, and it makes a dynamically smooth and time-dependent transition to terrain following in shallow coastal regions and to fixed pressure levels in the surface mixed layer and/or unstratified seas. In doing so, the model combines the advantages of the different coordinate types in simulating coastal and open ocean circulation features simultaneously (Chassignet et al. 2006).

The model domain (Fig. 1) extends from 28°S to the Fram Strait at 80°N with a horizontal resolution of $1/12°$ and a vertical resolution of 64 layers in σ_2 (which, unlike σ_θ, exhibits no density inversion in the Atlantic Ocean). The northern and southern boundaries are "vertical walls" with no normal flows. Within a buffer zone of 3° from these two boundaries, the model (potential) temperature θ and salinity S are restored to the monthly ocean climatology (Carnes 2009) with an e-folding time of 5–60 days, which increases with distance from the boundary. Thus, much of the model AMOC upwelling

occurs in the southern buffer zone. The simulation is integrated for 20 years with monthly climatological forcing from the 40-yr European Centre for Medium-Range Weather Forecasts Re-Analysis (ERA-40; Uppala et al. 2005). Because ocean convection is strongly influenced by synoptic weather systems and high-frequency winds are needed for a proper representation of the surface mixed layer physics (Kantha and Clayson 1994; Large et al. 1994), 3-hourly wind anomalies for year 2003, a year with neutral North Atlantic Oscillation (NAO), were added to the interpolated monthly means. The anomalies are based on the Fleet Numerical Meteorology and Oceanography Center 0.5° Navy Operational Global Atmospheric Prediction System (NOGAPS; Rosmond et al. 2002). The surface heat flux forcing includes the shortwave and longwave radiations that are directly from ERA-40, and the latent and sensible heat fluxes that are calculated using the model sea surface temperature (SST) and bulk formulas of Kara et al. (2005). Bulk formulas provide a negative feedback that increases (decreases) the net surface heat flux if the model SST is too cold (warm). The surface freshwater forcing includes evaporation, precipitation, and river runoffs. The model sea surface salinity (SSS) is also restored toward the monthly climatology with a restoring strength of 15 m per 30 days. The salinity difference (between model and climatology) in SSS restoring is clipped to be 0.5, to diminish its damping effect on ocean fronts; see Griffies et al. (2009) for a discussion. A simple energy loan parameterization is used for sea ice.

All diagnostics are performed on the last five years of the integration, which is representative of the circulation after spinup. The simulation reaches a statistical equilibrium in mean kinetic energy as well as in the volume transports of the AMOC and key western boundary currents (WBC) after 10 years. The model θ and S, on the other hand, are still adjusting (Xu et al. 2010, 2012, 2013) and would need several hundred years of integration to reach equilibrium.

3. Temperature–salinity structure of the North Atlantic circulation

In this section, we examine the modeled North Atlantic circulation through a variety of projections: 1) the traditional meridional overturning streamfunctions on depth and density coordinates, 2) the meridional volume transport on the θ–S plane, and 3) the streamfunctions with respect to θ and S that are integrated from the transport on the θ–S plane and are associated with the heat and freshwater transports. These projections describe different aspects of the circulation structure that can be compared to observations and other model results.
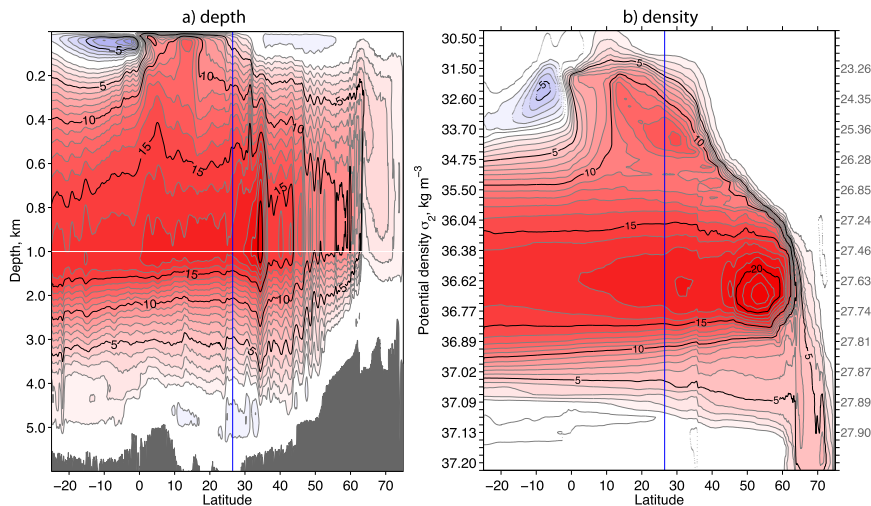
FIG. 2. Latitudinal distribution of the model mean meridional overturning streamfunction (Sv) with respect to z (km) and σ_2 (kg m^{-3}). Calculated as the integrated volume transport across the model zonal sections above depth/density. The gray numbers to the right denote the averaged σ_θ for each σ_2. The circulation is clockwise for positive streamfunctions, with northward flows in the upper and southward flows in the lower limb. Blue lines denote the location of the RAPID array at 26.5°N.

a. Meridional overturning streamfunctions with respect to depth and density

The AMOC is often visualized in meridional overturning streamfunctions with respect to depth ψ_z and density ψ_σ, defined as the meridional transport (Sv) across the basin above a constant depth z and isopycnal σ (here we use the model coordinate σ_2), respectively,

$$\psi_z(y,z) = \overline{\iint_{z' \leq z} v(x',y,z',t)\, dz'\, dx'},$$

$$\psi_\sigma(y,\sigma) = \overline{\iint_{\sigma' \leq \sigma} v(x',y,z',t)\, dz'\, dx'}, \quad (1)$$

where v is the meridional velocity, the overbar denotes a 5-yr average, and the x integration covers the entire span of the basin. The model streamfunctions are displayed in Figs. 2a and 2b. The ψ_z represents the vertical upwelling/sinking of the AMOC, whereas ψ_σ represents diapycnal water mass transformation, which converts the warm saline water in the northward upper limb into the cold fresh NADW in the southward lower limb (of the AMOC).

The ψ_z pattern in Fig. 2a shows that the strong equatorial upwelling brings about two-thirds of the northward AMOC transport to the top 50 m of the water column. The wind-driven Ekman transport is then able to drive a large seasonal variation of the AMOC (Xu et al. 2014) and the associated heat transport into this region. North of 35°N, the upper limb of the AMOC is below 100 m and the net transport near the surface is *southward* despite the

surface-intensified northward flowing Gulf Stream and North Atlantic Current (NAC).

As with ψ_z, the streamfunction ψ_σ (Fig. 2b) also exhibits a strong equatorial "upwelling." There are however significant differences. First, an overturning cell is seen in ψ_σ above 34.75 kg m^{-3} in the 10°–40°N latitude range, which corresponds to diapycnal water mass transformations in the subtropical gyre. This cell is made of northward-flowing western boundary current waters and slightly denser southward-flowing 18° Water (EDW, also called the Subtropical Mode Water). The magnitude of this overturning cell (~4 Sv in Fig. 2b) is consistent with the mean observed EDW formation rate of 3.3–4.0 Sv (Marsh 2000; Kwon and Riser 2004; LeBel et al. 2008). Second, the magnitude of the AMOC in ψ_z decreases northward as a function of latitude, whereas the ψ_σ streamfunction increases with latitude and exhibits a maximum value of 22 Sv near 53°N, ~5 Sv higher than that in the subtropics. This 5-Sv difference corresponds to Labrador Sea Water (LSW) that does not contribute to the larger-scale AMOC but instead "upwells" diapycnally within the latitude range 40°–52°N through strong subsurface interaction and mixing between the southward deep western boundary current (DWBC) and the northward NAC along the steep front in the western Newfoundland Basin.

The intensive RAPID observations at 26.5°N provide an excellent benchmark for assessing the model AMOC; see Xu et al. (2014) for a comparison on
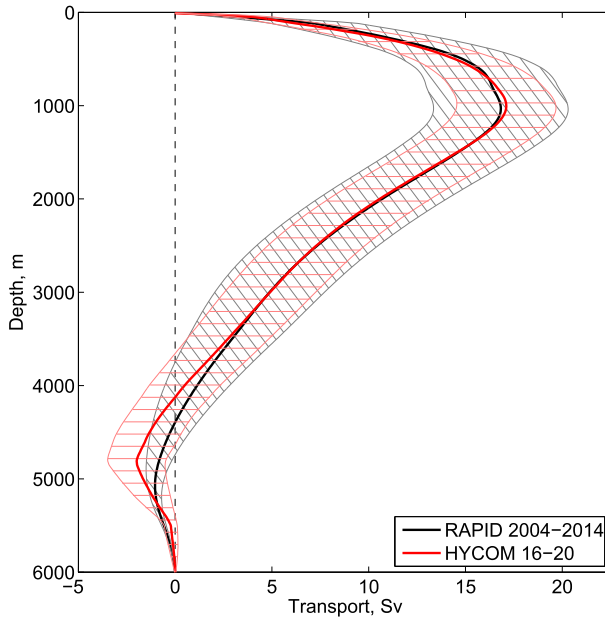
FIG. 3. A comparison of the observed and modeled meridional overturning streamfunction ψ_z (Sv) at 26.5°N. The observations are based on the latest RAPID results for the period April 2004–March 2014 [updated from McCarthy et al. (2015) and the references therein]; the model results are based on a climatologically forced eddy-resolving HYCOM simulation over a 5-yr period. The lines and hatched areas denote the mean and standard deviation values from monthly mean profiles, respectively.

temporal variability of various AMOC components. As displayed in Fig. 3, the model mean AMOC transport is 17.1 ± 2.6 Sv, compared to 16.9 ± 3.5 Sv in the RAPID results from 2004 to 2014 (updated from McCarthy et al. 2015, and references therein). The standard deviation values are based on monthly mean transports. The southward NADW transport extends from 1020 to 4140 m in the model, similar to 1030–4400 m in the RAPID results. The model NADW transports above and below 2500 m are 9.9 Sv and 7.2 Sv, respectively (9.5 and 7.4 Sv in the RAPID results, respectively). These two transports generally correspond to the LSW and Nordic seas overflow water (NSOW) contributions to the AMOC, and the values are in reasonable agreement with the long-term LSW and NSOW formation rates based on the observed CFC-11 inventories: 11.9 Sv and 7.9 Sv, respectively (LeBel et al. 2008).

The results in Figs. 2 and 3 can also be compared to other model results using similar horizontal resolutions; see Mielke (2015) and Marzocchi et al. (2015) for recent examples. One of the main differences between these studies (which were performed with global z-coordinate models) and ours is that no southward NADW transport is found deeper than

3000 m (4.9 Sv in RAPID and 4.8 Sv in HYCOM profiles in Fig. 3). Two factors may contribute to the unrealistic representation of the cold, dense NSOW in these simulations. First, retaining realistic water properties in the Nordic seas is more challenging in global models than in basin-scale models (in which the model θ and S are restored toward ocean climatology at the boundaries). Second, numerically induced diapycnal mixing arises in z-coordinate models because of advective truncation errors and horizontal diffusion tensors (Griffies et al. 2000), and that leads to a lighter and shallower NSOW (Legg et al. 2009). It is noteworthy that a large difference in the NADW constitutions not only impacts the time-mean AMOC structure and the heat transport, but also may change the nature of the variability, because the LSW and NSOW reflect different climate regimes: one is the subpolar North Atlantic and the other originates in the Nordic seas–Arctic Ocean.

b. Meridional transport on θ–S plane

The streamfunction ψ_σ depicts the meridional flow and the diapycnal water mass transformation by buoyancy forcing at the surface as well as the diapycnal mixing in the interior. A fuller picture that also includes the effects of isopycnic mixing and the related water mass transformation through "spice" change can be obtained by projecting the transbasin meridional transports on the θ–S plane, as $V(\theta, S)$ (e.g., Bailey et al. 2005; Langehaug et al. 2012),

$$V(\theta, S) = \frac{1}{\Delta\theta\Delta S} \overline{\iint_{|\theta'-\theta|\leq\Delta\theta/2, |S'-S|\leq\Delta S/2} v(x', y, z', t) \, dz' \, dx'}.$$
(2)

The unit of $V(\theta, S)$ is Sverdrups over an area in θ–S space, $\Delta\theta \times \Delta S$, which can be infinitesimal in principle. Figure 4 shows the model $V(\theta, S)$ at four selected sections in the Atlantic Ocean (black lines in Fig. 1), evaluated with $\Delta\theta \times \Delta S$ of 0.5°C × 0.1 psu. The northward-flowing upper limb of the AMOC ($\sigma_\theta < 27.65$ kg m^{-3}) warms from the equator to 26°N, as evidenced in the transport increase from the warmest water (above σ_θ of 24 kg m^{-3}), and then cools northward to the WOCE line AR19 and across the Greenland–Scotland Ridge. For the lower limb, although the overall θ–S values of NADW are similar from the AR19 line to the equator, significant warming takes place immediately south of the Greenland–Scotland Ridge in the NSOW ($\sigma \geq 27.80$ kg m^{-3}) due to entrainment mixing. The NSOW has a transport-weighted average θ of about 0.5°C in Fig. 4d, compared to 2.7°C in Figs. 4a–c.
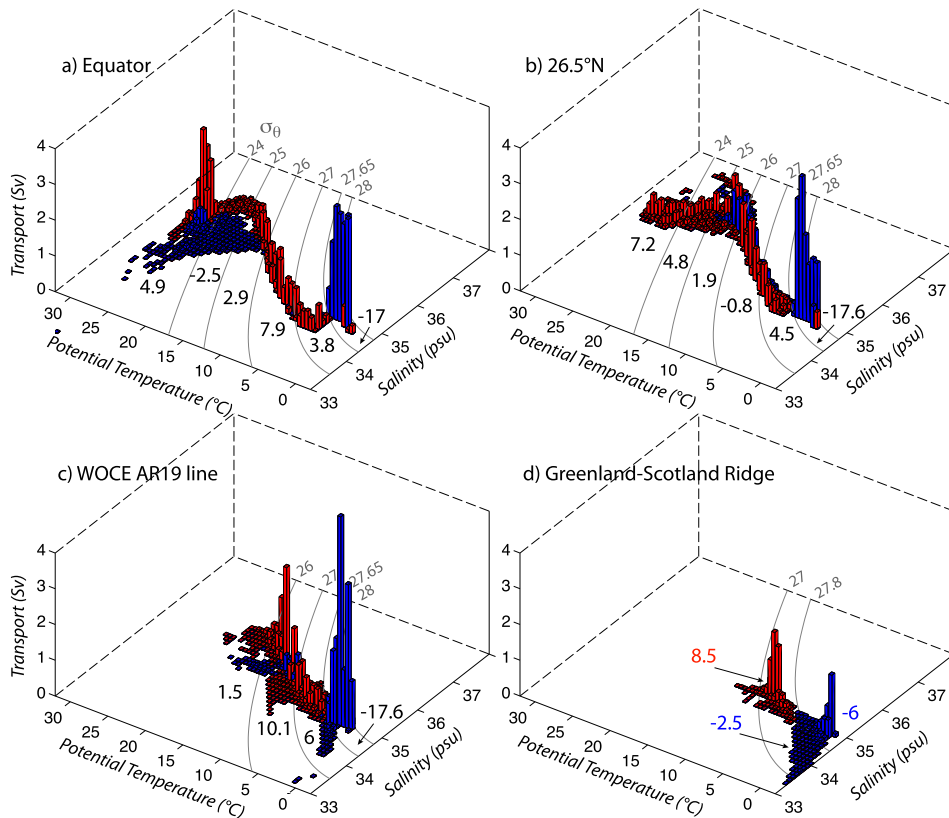
FIG. 4. (a)–(d) Model mean meridional transport projected onto the θ–S plane $V(\theta, S)$ across four transatlantic sections (black lines in Fig. 1). Red (blue) bars denote northward (southward) transports within a $\Delta\theta \times \Delta S$ box of 0.5°C × 0.1 psu [black numbers in (a)–(c) and are the net transport (Sv) for each σ_θ layer; red (blue) numbers in (d) are model northward (southward) transports for the three water masses defined in observations (e.g., Eldevik and Nilsen 2013).

Figure 4 also shows the meridional exchange of water masses with the same potential density σ yet different θ/S properties. This isopycnic spice exchange is invisible in streamfunction ψ_σ, which in essence is an integration of $V(\theta, S)$ along constant σ. For example, the model diapycnal overturning across the Greenland–Scotland Ridge is 7.5 Sv; but the full exchange involves a northward transport of warm saline Atlantic water (8.5 Sv) and two southward transports of fresh polar water (2.5 Sv) and dense NSOW (6 Sv) that are separated by σ_θ of 27.80 kg m^{-3} (Fig. 4d). This model result is essentially the same as the idealized thermohaline exchange based on observations (e.g., Hansen and Østerhus 2000; Hansen et al. 2008; Eldevik and Nilsen 2013), except that here all polar water returns to the North Atlantic east of Greenland because of the model configuration, whereas in observations some flows through the Davis Strait west of Greenland.

Across 26.5°N, the isopycnic exchange takes place primarily in the thermocline and it represents the spice change of the subtropical gyre seen in isopycnic space.

To illustrate this more clearly, the same $V(\theta, S)$ projection is evaluated in three different $\Delta\theta \times \Delta S$ bin resolutions in Fig. 5. A finer resolution allows the north-/southward transports with small $\Delta\theta$ and ΔS to be separated and better illustrates that, along isopycnals, the northward flow is slightly colder and fresher than the southward flow. This is consistent with the observed θ/S diagram at this latitude (Fig. 6): The water in the northward-flowing western boundary currents (denoted in red and orange dots) is colder and fresher than that in the southward return flow (blue dots). This spice exchange, as we discuss later, contributes to the heat and freshwater transports.

Although there is much detail in the three-dimensional θ/S transport diagrams, clusters of transport are clearly identifiable in $V(\theta, S)$ with known water masses, making a strong connection with classical hydrographic analysis of water masses. Furthermore, differencing the $V(\theta, S)$ transports between two latitudes, or within a box of latitude and longitude, can provide a quantitative description of water mass transformation.
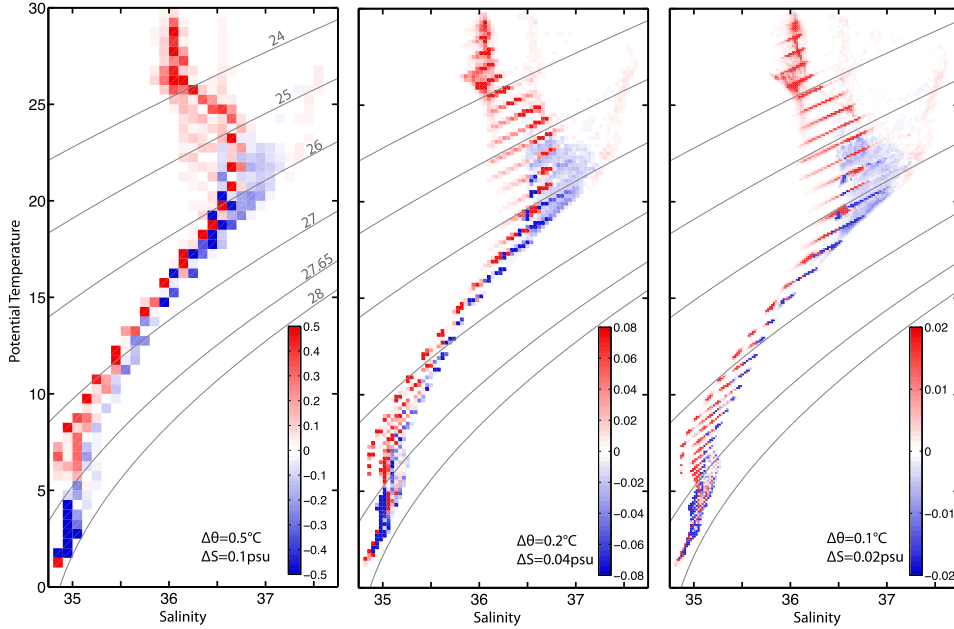
FIG. 5. Model mean meridional transport $V(\theta, S; \text{Sv})$ across 26.5°N evaluated in three $\Delta\theta \times \Delta S$ box resolutions. A finer resolution separates the northward (red) and southward (blue) flows with small water property differences in $\Delta\theta$ and ΔS.

c. Streamfunctions with respect to θ/S coordinates and their integrals

For consideration of ocean heat transport, Ferrari and Ferreira (2011) introduced a very useful diagnostic of the meridional streamfunction with respect to the θ coordinate, ψ_θ. It incorporates both the time-mean Eulerian transport and the eddy transport via the important bolus flux (the product of layer thickness and θ). The ψ_θ, as well as the streamfunction with respect to the salinity coordinate, ψ_S, can be obtained directly from integrating $V(\theta, S)$ along isotherms and isohalines:

$$\psi_\theta(y,\theta) = -\int_{\theta_{\min}}^{\theta} \int_{S_{\min}}^{S_{\max}} V(y,\theta',S')\, dS'\, d\theta',$$

$$\psi_S(y,S) = -\int_{S_{\min}}^{S} \int_{\theta_{\min}}^{\theta_{\max}} V(y,\theta',S')\, dS'\, d\theta'. \quad (3)$$

These are the same as time-averaged integrals from velocity v using definitions similar to Eq. (1):

$$\psi_\theta(y,\theta) = -\overline{\iint_{\theta' \leq \theta} v(x',y,z',t)\, dz'\, dx'},$$

$$\psi_S(y,S) = -\overline{\iint_{S' \leq S} v(x',y,z',t)\, dz'\, dx'}. \quad (4)$$

The meridional heat transport (MHT) and meridional freshwater transport (MFWT) can be conveniently

expressed as an integration of ψ_θ and ψ_S over full θ and S ranges (because of the zero net volume transport):

$$\text{MHT} \equiv \rho C_P \iint (\theta - \theta_0) V\, d\theta\, dS$$

$$= -\rho C_P \int_{\psi_\theta(\theta_{\min})}^{\psi_\theta(\theta_{\max})} (\theta - \theta_0)\, d\psi_\theta = \rho C_P \int_{\theta_{\min}}^{\theta_{\max}} \psi_\theta\, d\theta,$$

$$(5)$$

$$\text{MFWT} \equiv -\frac{1}{S_0} \iint (S - S_0) V\, d\theta\, dS$$

$$= \frac{1}{S_0} \int_{\psi_S(S_{\min})}^{\psi_S(S_{\max})} (S - S_0)\, d\psi_S = -\frac{1}{S_0} \int_{S_{\min}}^{S_{\max}} \psi_S\, dS,$$

$$(6)$$

in which ρ and C_P are the density and specific heat capacity of seawater, respectively, and $\rho C_P = 4.1 \times 10^6\,\mathrm{J\,m^{-3}\,K^{-1}}$ as in Johns et al. (2011); θ_0 and S_0 are the reference temperature and salinity, respectively; S_0 is also needed to convert the salinity transport into a freshwater transport and the value is set at 34.9 psu following Talley (2008). The unit for heat transport is PW and the same unit for volume transport (Sv) is used for freshwater transport, even though the meaning differs from the transport of seawater. Although $V(\theta, S)$ is sensitive to the $\Delta\theta$ and ΔS resolution (Fig. 5), its integrals ψ_θ and ψ_S are not and the three sets of $\Delta\theta \times \Delta S$ bins yield very similar streamfunctions (Fig. 7).
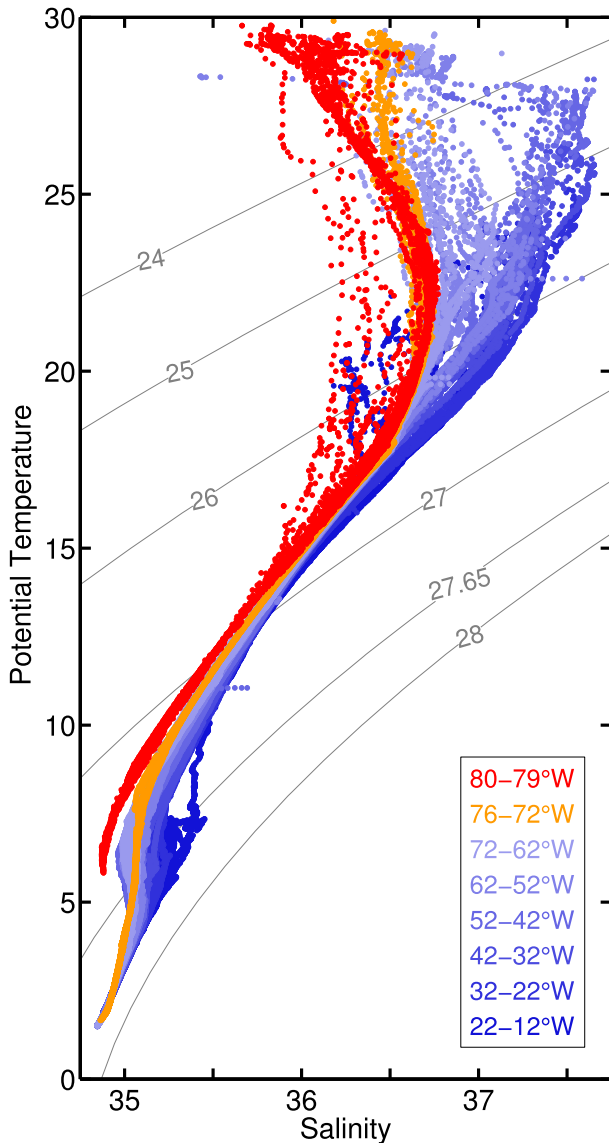
FIG. 6. Observed θ–S diagram based on the 1982 transatlantic hydrographic survey near 26°N (Roemmich and Wunsch 1985), color coded in longitude: red and orange dots denote profiles in the northward-flowing Florida Current (80–79°W) and Antilles Current (76–72°W) west and east of Abaco, Bahamas, respectively, whereas blue dots denote profiles in the southward return flow in the interior (east of 72°W).

This result shows that the diagnosis of heat and freshwater transports is insensitive to the $\Delta\theta \times \Delta S$ resolution.

The latitudinal distribution of model heat and freshwater transports is displayed in Figs. 8a and 8b, respectively, compared with Macdonald and Baringer (2013), Wijffels (2001), and Talley (2008). Most of these observational estimates are based on single or repeated hydrographic sections, and they exhibit significant uncertainties in representing the time-mean transports. The transports are considered well documented at two

locations. One location is 26.5°N, where the long-term continuous measurements of the RAPID array yield an 8.5-yr mean heat transport of 1.25 PW (McCarthy et al. 2015) and a freshwater divergence of −0.37 Sv between the Bering Strait and 26.5°N (McDonagh et al. 2015). The freshwater divergence implies an input of 0.37 Sv of freshwater from the atmosphere into the ocean to balance the southward freshwater transport across 26.5°N due to an exchange of water masses with different salinity. The model transports (1.25 PW and −0.38 Sv) are in excellent agreement with the observations. The other location is the Greenland–Scotland Ridge, where one can estimate heat (freshwater) transports of 0.31 PW (−0.14 Sv) based on the volume transports and θ/S values for the three water masses (Table 1 in Eldevik and Nilsen 2013). The model mean transport values of 0.29 PW/−0.14 Sv are in excellent agreement, as well.

The corresponding streamfunctions ψ_θ and ψ_S are displayed in Figs. 8c and 8d, respectively. The pattern of ψ_θ is generally similar to ψ_σ, except for a small shallow cell immediately north of the equator that is not seen in ψ_σ. The similarity between ψ_θ and ψ_σ is not surprising considering that the large-scale density stratification of the Atlantic (and most of the World Ocean) is primarily set by temperature. In the subpolar North Atlantic, the overturning is slightly higher in ψ_θ (than in ψ_σ), because it does not separate the cold fresh shelf water from NADW in the deep ocean. The ψ_S (Fig. 8d) differs greatly from ψ_θ and ψ_σ, owing to the nonmonotonic variation of salinity with depth. The signature of the large-scale AMOC can still be identified: In the upper limb, because of strong evaporation in the subtropics and precipitation in the intertropical convergence zone, the northward-flowing near-surface water undergoes large salinity changes from the South Atlantic to about 30°N. Farther north toward the subpolar North Atlantic, freshening (and cooling) dominates the upper-ocean transport. In the lower limb, the entire NADW layer is compressed into a very narrow S band close to 34.9 psu. Two counterclockwise cells with negative ψ_S can be seen in Fig. 8d: One is south of 20°N with $S < 34.9$ psu, representing the northward Antarctic Intermediate Water (AAIW), which returns southward as NADW; the other is in 10°–30°N with $S > 36$ psu, representing the subtropical North Atlantic gyre.

To establish the vertical structure of heat transport, Ferrari and Ferreira (2011) defined a heat function H as

$$H(y,\theta) \equiv \rho C_P \int_{\theta_{\min}}^{\theta} \psi_\theta(y,\theta')\, d\theta'. \qquad (7)$$

Since $H(\theta_{\max})$ is the total heat transport, its dependence on θ is supposed to represent an accumulation of the
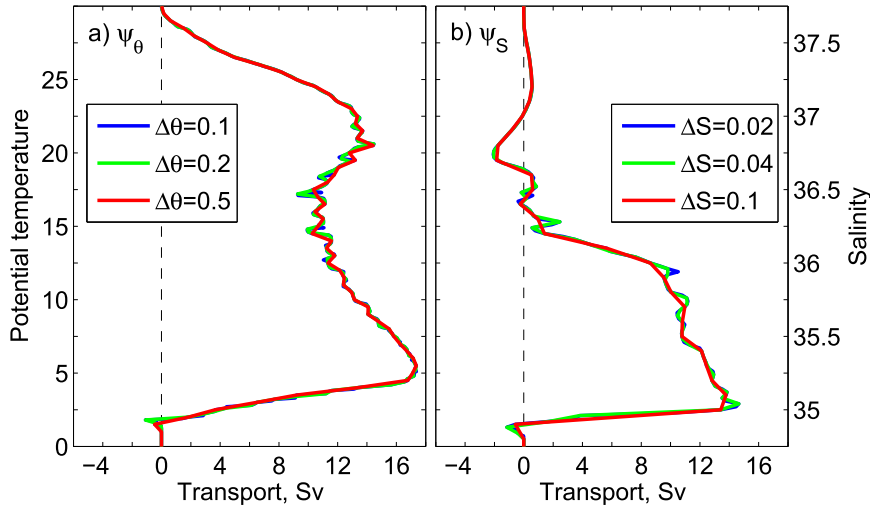
FIG. 7. Model mean streamfunctions (a) ψ_θ and (b) ψ_S at 26.5°N, integrated from $V(\theta, S)$ displayed in Fig. 5 using Eqs. (3) and (4). The results show that the streamfunctions are insensitive to the $\Delta\theta$ and ΔS resolutions used in $V(\theta, S)$.

heat transport contributions from the coldest to the warmest water masses. Figure 9a displays the $H(y, \theta)$ for our eddy-resolving simulation. Compared to Fig. 6b in Ferrari and Ferreira (2011), the $H(\theta_{\max})$ in the subtropical North Atlantic is 50% higher in our simulation, which is not too surprising, since their simulation uses a

much coarser resolution (which typically has more diffusive thermocline), and 0.3 PW is carried across the Greenland–Scotland Ridge into the Nordic seas (near zero in their model, meaning little NSOW). Otherwise, the pattern is similar: as H is accumulated upward, the entire NADW appears to contribute only ~0.1 PW to the
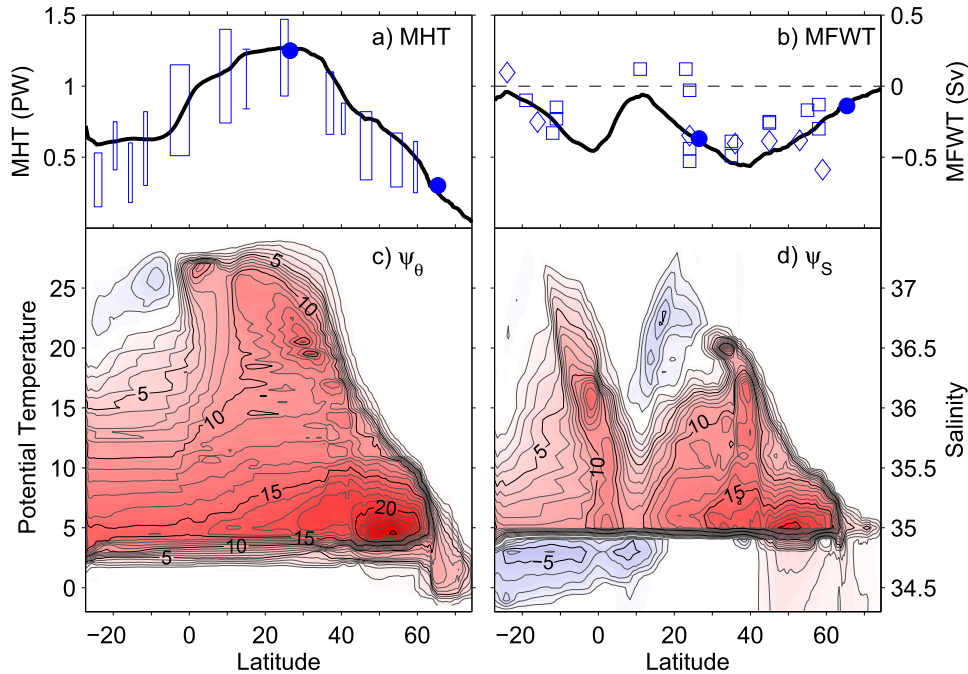
FIG. 8. Latitudinal distributions of the model (a) MHT (PW) and (b) MFWT (Sv) and the corresponding streamfunctions (c) ψ_θ and (d) ψ_S (Sv). Several observational estimates are included for comparison: rectangles and vertical bars are from Macdonald and Baringer (2013), squares and diamonds are from Wijffels (2001) and Talley (2008), filled blue dots are based on the RAPID data at 26.5°N (McCarthy et al. 2015; McDonagh et al. 2015), and the exchange across the Greenland–Scotland Ridge (Table 1 in Eldevik and Nilsen 2013).
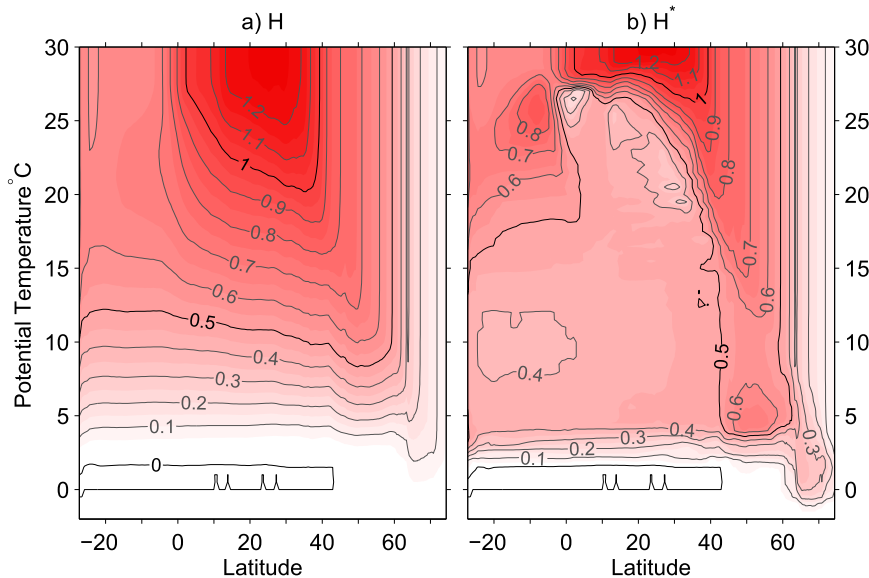
FIG. 9. Distributions of model heat function (PW) along latitude and potential temperature. The heat functions are defined as (a) $H = \rho C_p \int \psi_\theta \, d\theta$, following Ferrari and Ferreira (2011), and (b) $H^* = \rho C_p \int (\theta - \theta_0) \, d\psi_\theta$ with a reference temperature θ_0 of 10°C.

total heat transport. Thus, Ferrari and Ferreira (2011) suggest that the heat transport is surface intensified and this elevates the importance of wind-driven gyres in the upper ocean.

Heat function H is appealing in its simplicity, but it can be misleading with respect to the vertical structure of heat transport. The H contribution for a specific water mass, as defined in Eq. (7), depends on its θ range and ψ values, rather than on its volume transport $d\psi$ and θ values. Thus, 1) a water mass with uniform temperature (e.g., a "mode water") will contribute no heat transport at all, and 2) substantial heat transport can be attributed to depths where the meridional volume transport vanishes. The former explains why there is only a small contribution of NADW to the total heat transport, since its θ range (2°–5°C) is small compared to that for the upper limb (5°–30°C); the latter explains why a small ~4-Sv northward transport of 5°–22°C water contributes most of the heat transport at 26.5°N (Figs. 7a and 9a).

The main reason for the above-mentioned peculiar behavior of the function H is that, when the net volume transport is nonzero, it is not representative of the heat transport. The last two expressions in Eq. (5) are not equal and the MHT for an arbitrary θ, using integration by parts, should be written as

$$H^*(y, \theta) \equiv -\rho C_P \int_{\psi_\theta(\theta_{\min})}^{\psi_\theta(\theta)} (\theta' - \theta_0) \, d\psi_\theta(y, \theta')$$

$$= H(y, \theta) - \rho C_P (\theta - \theta_0) \psi_\theta(y, \theta). \qquad (8)$$

Compared to H, H^* includes an additional term that involves the net volume transport for water colder than θ and is dependent on reference temperature θ_0. The model H^* is displayed in Fig. 9b for a reference θ_0 of 10°C, which is roughly the transport-weighted mean temperature across the subtropical basin. The distribution of H^* exhibits a much higher contribution from NADW than does H (roughly 35% in the subtropics, rising to 60%–90% at subpolar latitudes), and it corrects the tendency of H to show contributions to meridional heat transport at depths where the meridional volume transport vanishes. However, its structure depends on the arbitrary choice of θ_0 and is therefore nonunique. In other words, while the heat function H^* is able to quantify some aspects of the heat transport structure, it cannot provide information on the relative importance of a specific water mass or circulation branch to the meridional heat transport. To achieve that, one needs to assess the sensitivity of the heat transport to the strength of the circulation branch in an ensemble of atmosphere–ocean simulations with widely varying overturning circulations and lateral gyres.

4. Heat and freshwater transports in the subtropical and subpolar North Atlantic

By parsing the meridional transport into its thermal and haline components in the previous section, we were able to identify using the transport on θ–S planes the distinct roles of overturning circulation and lateral gyres, which contrast diapycnal and spice-related isopycnic transport and mixing. In this section, we discuss
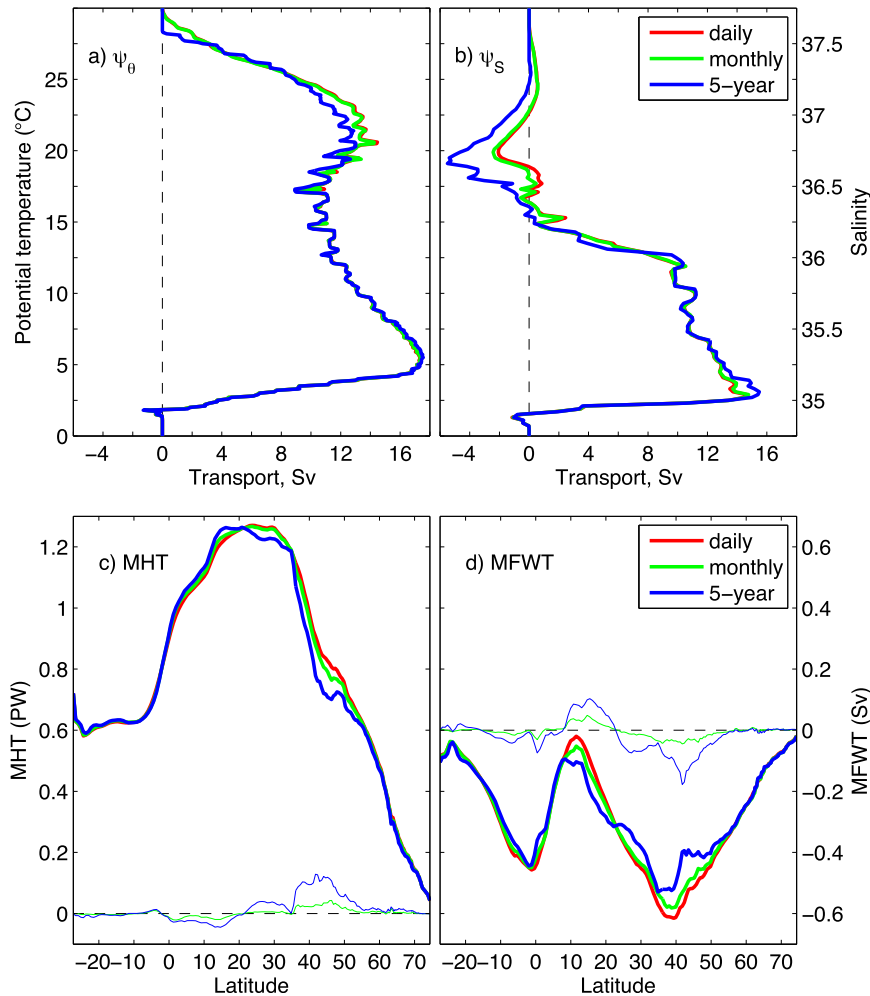
FIG. 10. (a),(b) Time-mean streamfunctions ψ_θ and ψ_S across 26.5°N and (c),(d) latitudinal distributions of the mean MHT and MFWT, calculated from daily mean, monthly mean, and 5-yr mean results. Thin lines in (c) and (d) represent time-mean MHT/MFWT contributions from temporal variability with a time scale shorter than 5 years (blue) and 1 month (green).

the contributions to the heat and freshwater transports in the subtropical and subpolar gyres by the time-mean and temporal dependent components, by the vertical and horizontal components, and finally by the diapycnal and isopycnal components.

a. Time mean versus temporal variability

The time-mean streamfunctions ψ_θ and ψ_S in Fig. 7 are calculated based on daily mean fields (velocity v, θ, and S) and then averaged over 5 years. In Figs. 10a and 10b, we compare the mean streamfunctions across 26.5°N computed from daily, monthly, and 5-yr means. The results show that the mean streamfunctions based on different time-mean fields are similar, suggesting that the heat and freshwater transports at this latitude are dominated by time-mean flow (note that interannual and longer-term variability is not considered in this

climatologically forced simulation). In particular, the results based on daily and monthly means are very similar, implying small contributions by temporal variability shorter than a month.

The latitudinal distribution of heat and freshwater transports (Figs. 10c and 10d) further shows the long-term mean circulation to be dominant throughout the Atlantic domain and the contributions from variability shorter than a month to be small (less than 0.04-PW heat and 0.05-Sv freshwater transports). Thus, for the remainder of this study, we calculate heat and freshwater transports based on monthly mean fields.

b. Heat and freshwater transports in the subtropical gyre

We decompose the model heat/freshwater transports across the 26.5°N into the classic vertical overturning and
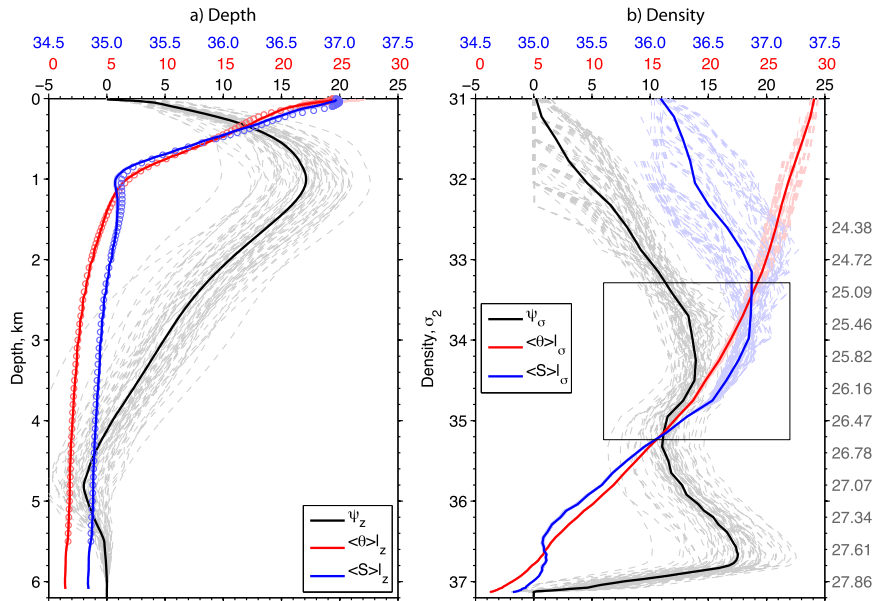
FIG. 11. Model overturning streamfunctions ψ (black) and zonally averaged profiles of potential temperature θ (red) and salinity S (blue) at 26.5°N, evaluated along z and σ_2 (the averaged σ_θ is listed in gray numbers to the right). Thick solid lines denote 5-yr mean and thin dashed lines denote monthly mean profiles. (a) The model monthly mean θ/S profiles vary only close to the surface and, for comparison, the observed profiles from the *World Ocean Atlas* (Locarnini et al. 2013; Zweng et al. 2013) are overlaid in circles. (b) The rectangle denotes the diapycnal cell seen in Fig. 2, which is largely Subtropical Mode Water convective overturning.

horizontal gyre components (e.g., Bryden and Imawaki 2001). The vertical component in Fig. 11a accounts for 88% or 1.10 ± 0.19 PW of the 1.24 ± 0.17-PW total heat transport, and the horizontal component in Fig. 12a for the remaining 12% (mean and standard deviation values are calculated from the 60 monthly mean transports). This vertical–horizontal partition is similar to the RAPID results (Johns et al. 2011; McCarthy et al. 2015). Johns et al. (2011) further pointed out that the Florida Current provides only 17%, whereas the midocean east of the Bahamas provides 83%, of this relatively small horizontal gyre contribution. The reason is that the θ deviation from the zonal mean has the opposite sign in the upper and lower parts of the Florida Current (thus their contributions nearly cancel). The model results exhibit a consistent distribution of θ deviation in Fig. 12a and a smaller contribution by the Florida Current (32%) than by the midocean (68%). For comparison, the two climate models in Msadek et al. (2013, see their Fig. 9) also exhibit a positive/negative θ deviation pattern that is somewhat similar to that observed in the Florida Current, but, because of a cold bias, these models are not able to get the positive θ deviation in the Antilles Current east of the Bahamas necessary for a northward heat transport by the horizontal component.

The modeled vertical overturning component leads to a freshwater transport of -0.71 ± 0.11 Sv, which is

nearly twice that of the total value (-0.37 ± 0.09 Sv). The horizontal gyre component transports a large amount of freshwater (0.34 Sv) northward, opposite of the action of vertical overturning. These model mean freshwater transport values are very similar to those of McDonagh et al. (2015) based on the RAPID observations: -0.78 and 0.35 Sv by the vertical and the horizontal components, respectively. Unlike the heat transports, the Florida Current accounts for all of the horizontal contributions and the midocean contributes a weak southward freshwater transport, consistent with the corresponding S deviation in Fig. 12a.

The thermocline/pycnocline tilts across the subtropical gyre at 26.5°N. The 15°C isotherm, as seen in Fig. 5 in Johns et al. (2011), is 500–600 m near the western boundary and 200 m at the eastern boundary and the western side of the Florida Strait. Thus, the vertical–horizontal decomposition mixes very different water masses by averaging the velocity, θ, and S zonally along constant depths. A similar decomposition by averaging along isopycnal surfaces avoids this, and the circulation can then be separated into a diapycnal overturning component and an isopycnic gyre component. The diapycnal component (in Fig. 11b) corresponds to heat and freshwater transports of 1.29 ± 0.18 PW and -0.53 ± 0.12 Sv, respectively. The isopycnal component (Fig. 12b) is responsible for a southward
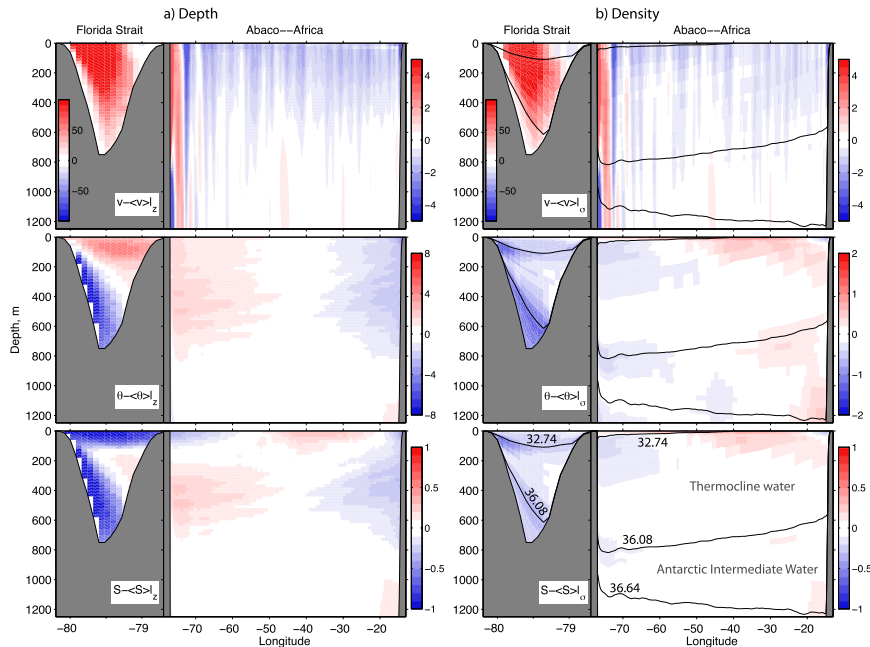
FIG. 12. Deviations of meridional velocity (cm s^{-1}), potential temperature (°C), and salinity from their zonal averages at 26.5°N, evaluated along (a) z and (b) σ_2. Black lines in (b) denote σ_2 interfaces used to separate the near-surface water (<32.74 kg m^{-3}), thermocline water (32.74–36.08), and AAIW (36.08–36.64). Note that the Florida Strait is enlarged and a different color scale is used for θ deviations between (a) and (b).

heat transport of 0.05 PW and a northward freshwater transport of 0.16 Sv across 26.5°N, because the northward flow is colder and fresher than the southward flow (see also Figs. 5 and 6).

The difference in transport contributions between the isopycnic and horizontal components (the latter of opposite sign for heat and a factor of 2 stronger for freshwater) can also be inferred from the θ/S deviations in Fig. 12. The Florida Current consists of three water masses of distinct origins that are distributed along strongly titled isopycnals (Fig. 13): the relatively fresh near-surface water ($\sigma_2 < 32.74$ kg m^{-3}) and AAIW ($\sigma_2 > 36.08$ kg m^{-3}) are the larger-scale AMOC components from the South Atlantic, whereas the saline thermocline water wedged in between is from the recirculating subtropical gyre. The accuracy of the modeled AMOC and subtropical gyre contributions will therefore strongly depend on the model's ability to represent these Florida Current finescale structures. The section at 26.5°N in the model compares well with observations in Fig. 13, especially the contrasting salinities as described above. The model Florida Current transport (30.2 Sv) is also close to the well-established value of 32 Sv in Meinen et al. (2010).

The subtropical gyre is responsible for most, if not all, of the isopycnal heat (-0.05 PW) and freshwater (0.16 Sv) transports. Only a small amount of diapycnal

heat (0.06 PW) and freshwater (-0.03 Sv) transports, associated with EDW mass transformations, takes place with the subtropical gyre (denoted by the rectangle in Fig. 11b). Thus, the heat/freshwater transports along and across isopycnals are of opposite signs and, when combined, the resulting heat transport associated with the subtropical gyre is close to 0 PW and the freshwater transport is close to 0.13 Sv northward. The magnitude of the latter is about one-third of the total freshwater transport (0.37 Sv southward) across 26.5°N.

The 0-PW heat transport associated with the subtropical gyre contrasts strongly with the 0.4 PW derived by Talley (2003). The 0.4 PW is determined by contrasting the heat transports in the southward component of the subtropical gyre and in the northward flow [near-surface water transport in the Florida Current and Ekman transport; see Fig. 3a in Talley (2003) for details]. The same calculation, performed using the model outputs, gives a similar value for the heat transport (0.55 PW). However, we argue here that this value does not truly represent the heat transport contribution of the subtropical gyre because the near-surface layer in the Florida Current is dominated by relatively freshwater from the tropical/South Atlantic (Fig. 13) and is best regarded as part of the larger-scale AMOC. To address the latter point, we refine Talley's (2003) calculation by dividing the upper-ocean transport into the three layers
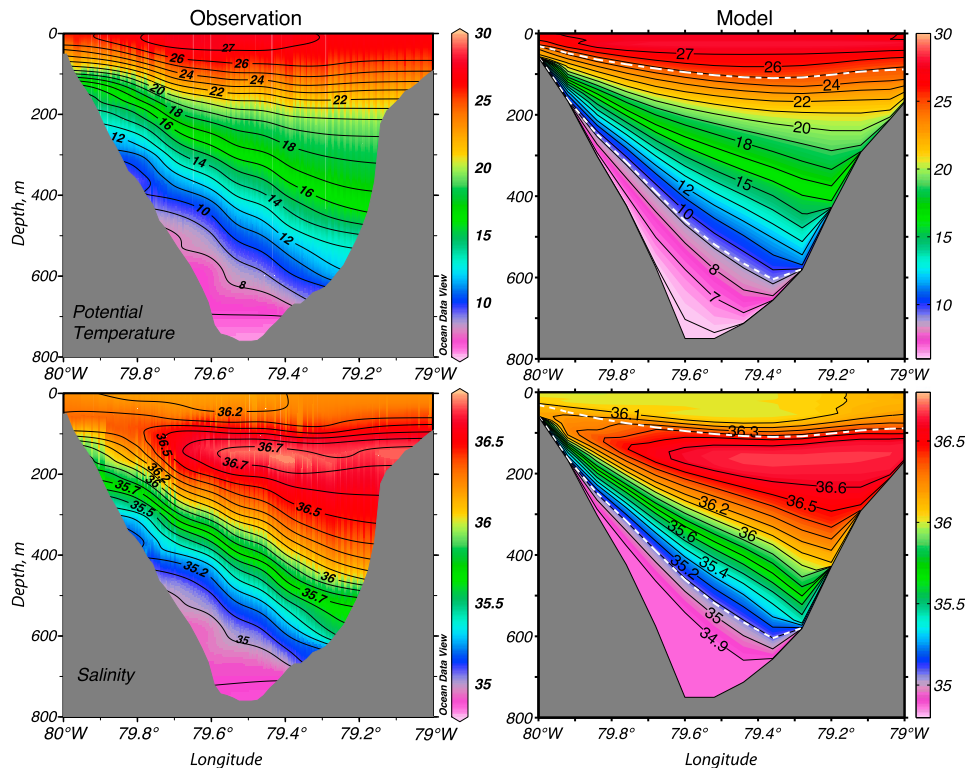
FIG. 13. Distribution of potential temperature and salinity across the Florida Current near 26°N. The observed sections are based on CTD profiles over 1982–2007 available in the World Ocean Database. The model results are based on a 5-yr mean HYCOM simulation (years 16–20). The dashed white lines denote σ_2 interfaces of 32.74 and 36.08 kg m^{-3} as shown in Fig. 12b.

corresponding to the fresh near-surface water, thermocline water, and AAIW as illustrated in Figs. 12 and 13. The transport pattern in Fig. 14 shows that the fresh near-surface water and the AAIW exhibit no southward return flow, whereas the thermocline water is mostly confined within the recirculating subtropical gyre. This pattern is consistent with the salinity distribution (Fig. 13) and the attribution of water masses to the AMOC and the subtropical gyre. The subtropical gyre contributions to the heat and freshwater transports, calculated from this thermocline layer, are about 0 PW and 0.11 Sv, respectively and are consistent with the subtropical gyre contributions derived from the diapycnal–isopycnic decomposition as discussed above.

The 0-PW gyre heat transport also contrasts with the results of Ferrari and Ferreira (2011), who concluded that the subtropical gyre could contribute about 40% of the total heat transport. The percentage was inferred by comparing the heat transports in two simulations, one with and one without the AMOC. Such inference is valid as long as the subtropical gyres remain similar in the two simulations. This is clearly not the case, however, since the gyre in the simulation without an AMOC exhibits a much higher subtropical gyre diapycnal overturning cell

than in the simulation with the AMOC [see Figs. 6 and 12 in Ferrari and Ferreira (2011) for details].

c. Heat and freshwater transports in the subpolar gyre

Here we contrast the heat and freshwater transports in the subpolar North Atlantic to that of the subtropics by applying the above-mentioned decompositions to a section near 58°N (red line, Fig. 1) that extends from southeast of Cape Farewell, Greenland, to Scotland. Its location is close to repeated hydrographic sections (Sarafanov et al. 2012), repeat ADCP sections for the upper 400 m (Chafik et al. 2014), and the recently deployed transbasin mooring line as part of the Overturning in the Subpolar North Atlantic Program (OSNAP, www.o-snap.org). In the model, the total mean heat and freshwater transports across this section are 0.43 ± 0.024 PW and −0.20 ± 0.027 Sv, respectively. There are only limited observational estimates of the heat and freshwater transports near 58°N and the values range from 0.25 to 0.61 PW and from −0.13 to −0.59 Sv, respectively (Fig. 8).

As was done for the 26.5°N section (Figs. 11 and 12), we decompose the circulation into a vertical (diapycnal) overturning (Fig. 15) and horizontal (isopycnic) gyre
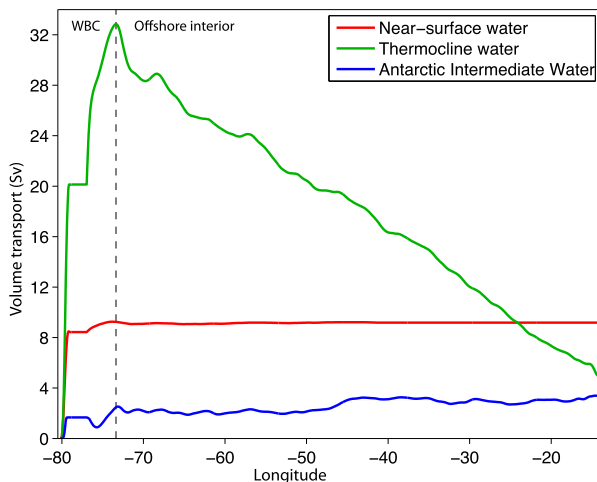
FIG. 14. Eastward accumulation of mean meridional volume transport at 26.5°N for the three water masses above the σ_2 interface of 36.64 kg m^{-3} (see Figs. 12b and 13). The near-surface water and the AAIW are AMOC components from the South Atlantic and exhibit no return flow, whereas the thermocline water mostly recirculates within the subtropical gyre. The dashed vertical line indicates the separation between the WBC and the offshore interior.

(Fig. 16) components. At 58°N, the isopycnals exhibit a steeper slope across the basin than at 26.5°N and the flows are more barotropic. As a result, the vertical overturning ψ_z, 8.2 ± 1.30 Sv, is only half of the value of the diapycnal overturning ψ_σ, 16.4 ± 2.48 Sv. The zonally averaged profiles of θ and S also differ significantly between the two decompositions: Averaged along z levels, the water in the northward limb (above 800 m) is colder and fresher than 10°C and 35.2 psu, whereas along σ surfaces, more than 12 Sv of the northward limb has θ and S in the ranges of 10°–12°C and 35.2–35.4 psu (Fig. 15), respectively. These differences in streamfunctions and profiles of θ and S lead to large differences in the heat and freshwater transports: 0.14 ± 0.032 PW and 0.06 ± 0.013 Sv for the z-based overturning compared to 0.43 ± 0.027 PW and −0.19 ± 0.017 Sv for the diapycnal overturning. Thus, the vertical overturning accounts for only about one-third of the total heat and freshwater transports, whereas the diapycnal overturning essentially accounts for all of the heat and freshwater transports.

The result that the isopycnic gyre contributes little to heat and freshwater transports may at first appear surprising, given the large θ and S difference across the 58°N section, the strong subpolar gyre, and the large zonally varying air–sea fluxes. In Fig. 17, we show the zonal structure of the volume transport across this section for five density layers (see Fig. 16b for the depth of the isopycnal surfaces), which correspond to the key

water masses of the region: the modified North Atlantic water (MNAW), subpolar mode water (SPMW), LSW, Iceland–Scotland overflow water (ISOW), and Denmark Strait overflow water (DSOW). The MNAW flows northward across the section east of 30°W, primarily in three branches: near 24°W along the deep part of the Iceland Basin, near 12°W in the Rockall Channel, and 21–16°W over the Hatton Bank. These patterns are generally consistent with the observations (Sarafanov et al. 2012; Chafik et al. 2014). Three of the water masses (MNAW, SPMW, and LSW) recirculate west of 25°W (3.7, 5, and 15 Sv, respectively). In all cases, the differences in θ and S are very small (Fig. 16b), resulting in a negligible isopycnic contribution to heat and freshwater transports. As a result, the heat and freshwater transports across this section are dominated by the diapycnal water mass transformation associated with the larger-scale AMOC: 16.4 Sv of MNAW across this latitude are transformed into 7.0 Sv of SPMW, 2.0 Sv of LSW, and 7.4 Sv of NSOW (evenly split between ISOW and DSOW). Using the repeat hydrographic sections, Sarafanov et al. (2012) also obtain a similar value (16.5 Sv) for the larger-scale AMOC but with a significantly higher NSOW transport (13.3 Sv) than in the model. However, there are still uncertainties in the NSOW transport and a much lower value of 9 Sv was computed by Bacon and Saunders (2010) using a yearlong current meter array near 59°N. The difference between the model and the observations may be due to a lower entrainment mixing in the ISOW and DSOW.

5. Summary and discussion

Large-scale circulations, such as the Atlantic meridional overturning circulation (AMOC) and the wind-driven gyres, play an important role in the earth's climate system by carrying, redistributing heat and freshwater through ocean basins, and interacting with the atmosphere. Motivated in part by ongoing discussions regarding the AMOC and subtropical gyre's contributions to the meridional oceanic heat transport near 25°N, we perform a detailed examination of the circulation structure and the water mass properties in a high-resolution numerical ocean model and quantify the relative role of different circulation components in the North Atlantic heat and freshwater transports. The key results are as follows:

1) The meridional transport streamfunction with respect to density (ψ_σ) describes the diapycnal transformation of the circulation and exhibits notable subbasin-scale meridional overturning cells for the Subtropical Mode Water and Labrador Sea Water, in the subtropical and subpolar gyres, respectively. These gyre-scale overturning cells are not shown in the streamfunction with
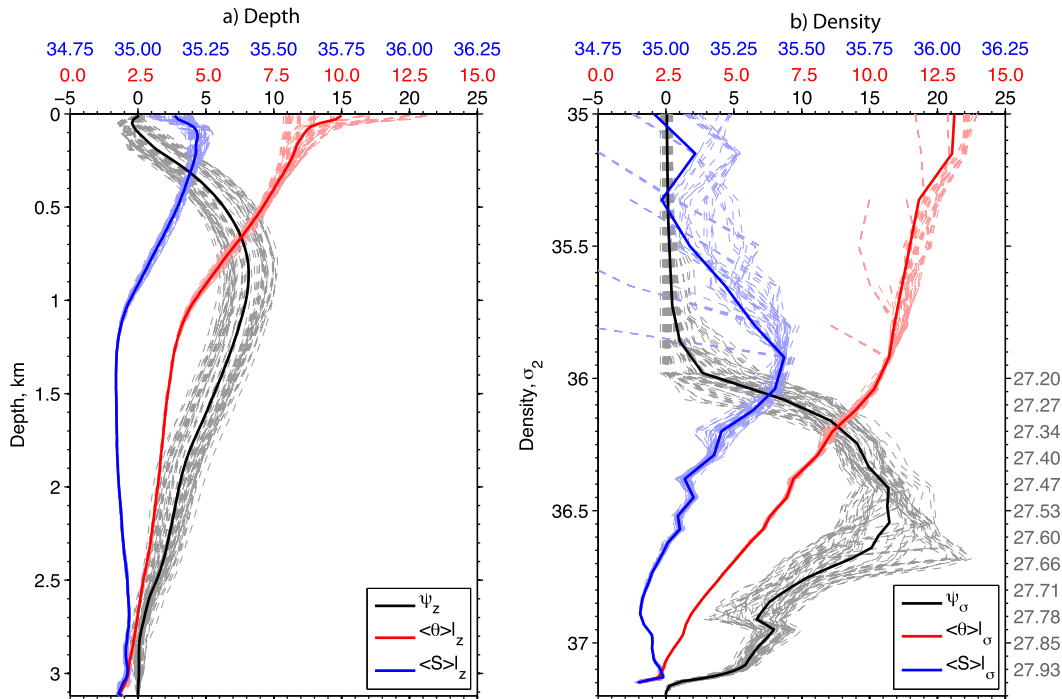
FIG. 15. Model overturning streamfunctions ψ (black) and zonally averaged profiles of θ (red) and S (blue) near 58°N, evaluated along z and σ_2 (σ_θ is listed in gray numbers to the right). The section runs from Cape Farewell to Scotland (red line in Fig. 1). Thick solid lines denote 5-year mean and thin dashed lines denote monthly mean profiles.

respect to depth (ψ_z). In the subtropical North Atlantic, one can think of three circulation components: the diapycnal overturning and isopycnal recirculation of the subtropical gyre, as well as the large-scale AMOC. The wind stress is intimately connected with all three components and "drives" both the isopycnal gyre through Ekman pumping and the diapycnal overturning via the air–sea buoyancy fluxes.

2) The meridional volume transports projected onto the potential temperature–salinity (θ–S) plane provide a comprehensive summary of the mass, heat, and salt (freshwater) transports across a given latitude. The width of the transport projection along isopycnal curves (the "spice") controls the contribution of isopycnal heat and freshwater transports. Divergence of adjacent sections describes the water mass transformation of the enclosed area, which balances the air–sea heat and freshwater fluxes and the subsurface mixing in the interior. It should be noted that these transbasin transports projected onto a θ–S plane differ from the streamfunctions on the θ–S plane as defined in Nycander et al. (2007), Döös et al. (2012), and Zika et al. (2012, 2013). The latter streamfunctions are more analogous to the thermodynamic analysis on the pressure–volume plane for a gas undergoing cyclic exchanges of heat

and work, without regard to spatial transport and transformation, which are the subject of this study.

3) The meridional streamfunction with respect to the θ and S coordinates (ψ_θ and ψ_S, respectively), which can be directly integrated from the transport on the θ–S plane, describes the meridional circulation in temperature and salinity classes, respectively. Ferrari and Ferreira (2011) extended the ψ_θ and defined a heat function with the aim of finding contributions of heat transport in terms of θ. Their heat function definition [Eq. (7)] exhibits the peculiar property that a water mass with uniform θ has no heat transport contribution, regardless of its volume transport. This leads to the impression that insignificant heat transport is contributed by NADW, which has a narrow θ range of 2°–4°C. The full expression of heat function [Eq. (8)] corrected this, but its distribution does depend on the choice of reference temperature. To fully determine the relative importance of a water mass or circulation branch in the heat transport, one would need to consider the variability. For example, Frajka-Williams et al. (2016) show that the AMOC transport variability at 26.5°N (highly correlated with the heat transport variability) is dominated by the variability in the lower part of the NADW below 3000 m.
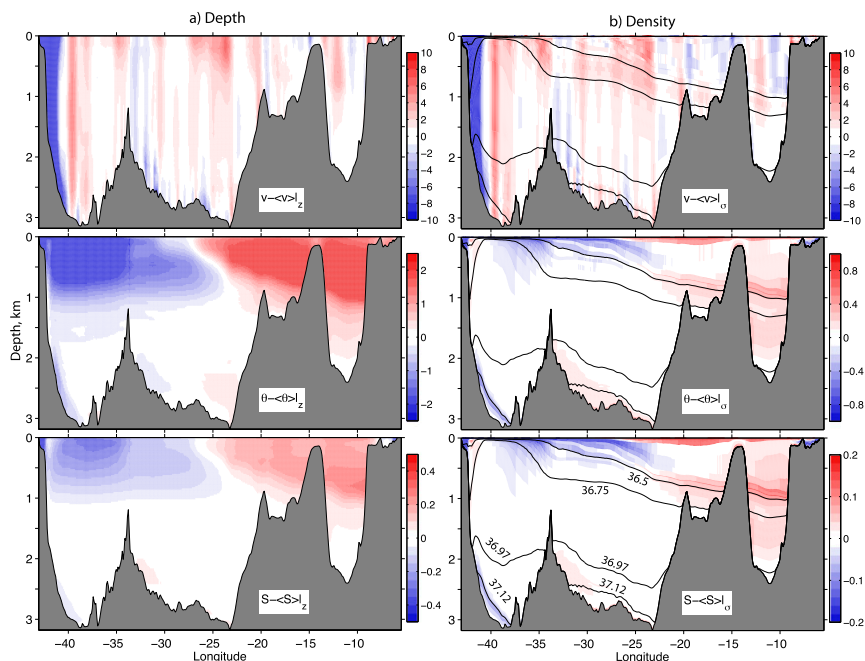
FIG. 16. Deviations of meridional velocity (cm s^{-1}), potential temperature (°C), and salinity from their zonal averages, evaluated along (a) constant depth and (b) density, at the model section near 58°N. Black contours in (b) denote σ_2 (kg m^{-3}) interfaces that divide the water column into five layers of water mass (see Fig. 17 for transports).

4) At 26.5°N in the subtropics, the traditional vertical–horizontal decomposition of the model circulation leads to the horizontal component being responsible for a northward heat transport of 0.14 PW, which is 12% of the total heat transport, and a northward freshwater transport of 0.34 Sv, which is opposite of the total southward freshwater transport of 0.37 Sv. These vertical and horizontal components do not exactly correspond to the AMOC and the wind-driven subtropical gyre, however. The subtropical gyre consists of a "shallow" diapycnal overturning cell and an isopycnic recirculation gyre that transport heat and freshwater in opposite directions. When combined, the two components cancel out and the subtropical gyre contributes about 0 PW heat transport. The subtropical gyre, however, contributes a northward freshwater transport of 0.13 Sv, compared to the 0.5-Sv southward AMOC freshwater transport (note that these two opposite transports have different roles: one is to balance the evaporation within the subtropical gyre, the other is to balance the overall precipitation in the subpolar North Atlantic and Nordic seas–Arctic Ocean). Consistent heat and freshwater transports are obtained when the northward and southward components of the subtropical gyre are examined following Talley's (2003) approach, with the layered structure of the circulation being considered.

5) Near 58°N in the subpolar North Atlantic, the diapycnal component (of the circulation) results from the transformation of the warm saline water in the upper layer into the colder fresher water and accounts for essentially all the heat and freshwater transports. In contrast, the vertical component is responsible for only one-third of the heat and freshwater transports. This result underscores the need to map the spatial distribution and to understand the driving processes of the (diapycnal) water mass transformation in the subpolar region, in both observations and numerical models.

The results are based on one climatologically forced Atlantic model and its robustness needs to be further examined in other models. It is essential that the models are able to represent well the observed circulation patterns and water mass distributions, since the model AMOC versus gyre contributions to the heat and freshwater transports will depend on the model's ability to represent these detailed circulation patterns and water mass distributions. This is a challenge not only for a low-resolution coupled climate model, in which mescoscale dynamics are not resolved and the model water properties typically exhibit large biases (Msadek et al. 2013), but also for atmospherically
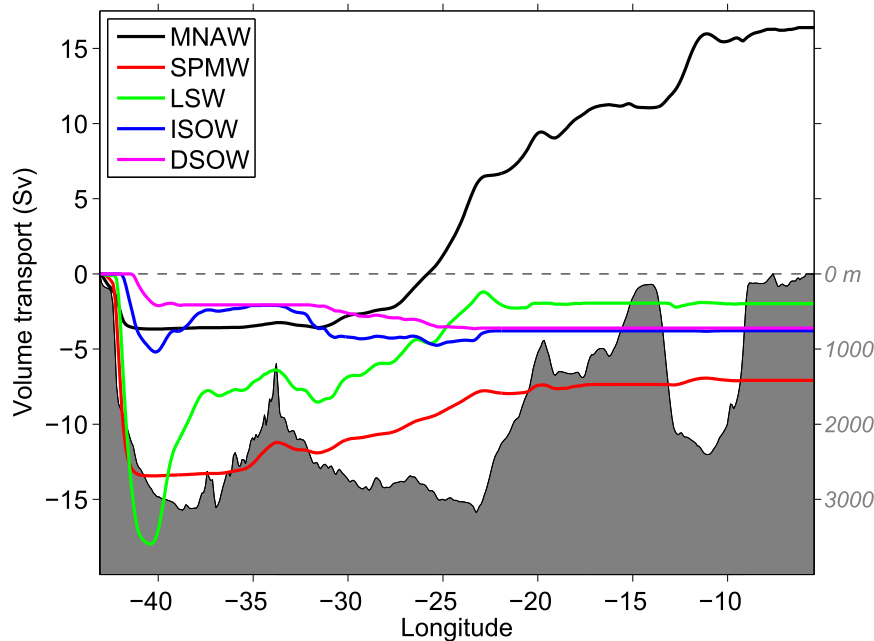
FIG. 17. Eastward accumulation of the meridional volume transport across the model section near 58°N in five layers (see Fig. 16b for interface depths), representing the MNAW ($\sigma_2 < 36.5\,\mathrm{kg\,m^{-3}}$), SPMW ($36.5 \leq \sigma_2 < 36.75$), LSW ($36.75 \leq \sigma_2 < 36.97$), ISOW ($36.97 \leq \sigma_2 < 37.12$), and DSOW ($\sigma_2 \geq 37.12$). The gray shading shows the bottom bathymetry.

forced ocean general circulation models at eddying resolutions. As discussed in Johns et al. (2011), there has been a general tendency in ocean models to underestimate the heat transport near 26.5°N in the Atlantic, even with a mean AMOC transport comparable to observations. The model results presented in this study are shown to be in good agreement at key observed locations with the observed circulation structure and water mass distribution. In particular, both the AMOC and the heat/freshwater transports at 26.5°N are consistent with the RAPID results. One should remain cautious, however, that the good agreement may be attributed in part to the basin-scale model configuration details (e.g., boundary restoring to climatology) and further comparisons to long-term global simulations are needed.

REFERENCES

Bacon, S., and P. M. Saunders, 2010: The deep western boundary current at Cape Farewell: Results from a moored current meter array. *J. Phys. Oceanogr.*, **40**, 815–829, doi:10.1175/2009JPO4091.1.

Bailey, D. A., P. B. Rhines, and S. Häkkinen, 2005: Formation and pathways of North Atlantic Deep Water in a coupled ice–ocean model of the Arctic–North Atlantic Oceans. *Climate Dyn.*, **25**, 497–516, doi:10.1007/s00382-005-0050-3.

Bleck, R., 2002: An oceanic general circulation model framed in hybrid isopycnic-Cartesian coordinates. *Ocean Modell.*, **4**, 55–88, doi:10.1016/S1463-5003(01)00012-9.

Bryden, H. L., and S. Imawaki, 2001: Ocean heat transport. *Ocean Circulation and Climate: Observing and Modelling the Global Ocean*, G. Siedler, J. Church, and J. Gould, Eds., International Geophysics Series, Vol. 77, Academic Press, 455–474.

Carnes, M. R., 2009: Description and evaluation of GDEM-V3.0. Naval Research Laboratory Memo. Rep. NRL/MR/7330–09-9165, 21 pp. [Available online at http://www7320.nrlssc.navy.mil/pubs/2009/carnes-2009.pdf.]

Chafik, L., T. Rossby, and C. Schrum, 2014: On the spatial structure and temporal variability of poleward transport between Scotland and Greenland. *J. Geophys. Res. Oceans*, **119**, 824–841, doi:10.1002/2013JC009287.

Chassignet, E. P., L. T. Smith, G. R. Halliwell, and R. Bleck, 2003: North Atlantic simulations with the Hybrid Coordinate

Ocean Model (HYCOM): Impact of the vertical coordinate choice, reference pressure, and thermobaricity. *J. Phys. Oceanogr.*, **33**, 2504–2526, doi:10.1175/1520-0485(2003)033<2504:NASWTH>2.0.CO;2.

——, and Coauthors, 2006: Generalized vertical coordinates for eddy-resolving global and coastal ocean forecasts. *Oceanography*, **19** (1), 118–129, doi:10.5670/oceanog.2006.95.

Döös, K., J. Nilsson, J. Nycander, L. Brodeau, and M. Ballarotta, 2012: The World Ocean thermohaline circulation. *J. Phys. Oceanogr.*, **42**, 1445–1460, doi:10.1175/JPO-D-11-0163.1.

Eldevik, T., and J. E. Ø. Nilsen, 2013: The Arctic–Atlantic thermohaline circulation. *J. Climate*, **26**, 8698–8705, doi:10.1175/JCLI-D-13-00305.1.

Ferrari, R., and D. Ferreira, 2011: What processes drive the ocean heat transport? *Ocean Modell.*, **38**, 171–186, doi:10.1016/j.ocemod.2011.02.013.

Frajka-Williams, E., and Coauthors, 2016: Compensation between meridional flow components of the Atlantic MOC at 26°N. *Ocean Sci.*, **12**, 481–493, doi:10.5194/os-12-481-2016.

Griffies, S. M., R. C. Pacanowski, and R. W. Hallberg, 2000: Spurious diapycnal mixing associated with advection in a *z*-coordinate ocean model. *Mon. Wea. Rev.*, **128**, 538–564, doi:10.1175/1520-0493(2000)128<0538:SDMAWA>2.0.CO;2.

——, and Coauthors, 2009: Coordinated Ocean-ice Reference Experiments (COREs). *Ocean Modell.*, **26**, 1–46, doi:10.1016/j.ocemod.2008.08.007.

Hall, M. M., and H. L. Bryden, 1982: Direct estimates and mechanisms of ocean heat transport. *Deep-Sea Res.*, **29A**, 339–359, doi:10.1016/0198-0149(82)90099-1.

Hansen, B., and S. Østerhus, 2000: North Atlantic–Nordic Seas exchanges. *Prog. Oceanogr.*, **45**, 109–208, doi:10.1016/S0079-6611(99)00052-X.

——, ——, W. R. Turrell, S. Jønsson, H. Valdimarsson, H. Hátún, and S. M. Olsen, 2008: The inflow of Atlantic water, heat, and salt to the Nordic seas across the Greenland–Scotland ridge. *Arctic-Subarctic Ocean Fluxes: Defining the Role of the Northern Seas in Climate*, R. R. Dickson, J. Meincke, and P. B. Rhines, Eds., Springer, 15–43, doi:10.1007/978-1-4020-6774-7_2.

Herweijer, C., R. Seager, M. Winton, and A. Clement, 2005: Why ocean heat transport warms the global mean climate. *Tellus*, **57A**, 662–675, doi:10.1111/j.1600-0870.2005.00121.x.

Holland, M. M., C. M. Bitz, and B. Tremblay, 2006: Future abrupt reductions in the summer Arctic sea ice. *Geophys. Res. Lett.*, **33**, L23503, doi:10.1029/2006GL028024.

Johns, W. E., and Coauthors, 2011: Continuous, array-based estimates of Atlantic Ocean heat transport at 26.5°N. *J. Climate*, **24**, 2429–2449, doi:10.1175/2010JCLI3997.1.

Kang, S. M., I. M. Held, D. M. Frierson, and M. Zhao, 2008: The response of the ITCZ to extratropical thermal forcing: Idealized slab-ocean experiments with a GCM. *J. Climate*, **21**, 3521–3532, doi:10.1175/2007JCLI2146.1.

——, R. Seager, D. M. W. Frierson, and X. Liu, 2015: Croll revisited: Why is the northern hemisphere warmer than the southern hemisphere? *Climate Dyn.*, **44**, 1457–1472, doi:10.1007/s00382-014-2147-z.

Kantha, L. H., and C. A. Clayson, 1994: An improved mixed layer model for geophysical applications. *J. Geophys. Res.*, **99**, 25 235–25 266, doi:10.1029/94JC02257.

Kara, A. B., H. E. Hurlburt, and A. J. Wallcraft, 2005: Stability-dependent exchange coefficients for air–sea fluxes. *J. Atmos. Oceanic Technol.*, **22**, 1080–1094, doi:10.1175/JTECH1747.1.

Kwon, Y.-O., and S. C. Riser, 2004: North Atlantic Subtropical Mode Water: A history of ocean-atmosphere interaction

1961–2000. *Geophys. Res. Lett.*, **31**, L19307, doi:10.1029/2004GL021116.

Langehaug, H. R., I. Medhaug, T. Eldevik, and O. H. Otterå, 2012: Arctic/Atlantic Exchanges via the Subpolar Gyre. *J. Climate*, **25**, 2421–2439, doi:10.1175/JCLI-D-11-00085.1.

Large, W. G., J. C. McWilliams, and S. C. Doney, 1994: Ocean vertical mixing: A review and a model with a nonlocal boundary layer parameterization. *Rev. Geophys.*, **32**, 363–403, doi:10.1029/94RG01872.

LeBel, D. A., and Coauthors, 2008: The formation rate of North Atlantic Deep Water and Eighteen Degree Water calculated from CFC-11 inventories observed during WOCE. *Deep-Sea Res. I*, **55**, 891–910, doi:10.1016/j.dsr.2008.03.009.

Legg, S., and Coauthors, 2009: Improving oceanic overflow representation in climate models: The Gravity Current Entrainment Climate Process Team. *Bull. Amer. Meteor. Soc.*, **90**, 657–670, doi:10.1175/2008BAMS2667.1.

Locarnini, R. A., and Coauthors, 2013: *Temperature.* Vol. 1, *World Ocean Atlas 2013*, NOAA Atlas NESDIS 73, 40 pp.

Macdonald, A. M., and M. O. Baringer, 2013: Ocean heat transport. *Ocean Circulation and Climate: A 21st Century Perspective*, G. Siedler et al., Eds., International Geophysics Series, Vol. 103, Academic Press, 759–786, doi:10.1016/B978-0-12-391851-2.00029-5.

Marsh, R., 2000: Recent variability of the North Atlantic thermohaline circulation inferred from surface heat and freshwater fluxes. *J. Climate*, **13**, 3239–3260, doi:10.1175/1520-0442(2000)013<3239:RVOTNA>2.0.CO;2.

Marzocchi, A., J. J.-M. Hirschi, N. P. Holliday, S. A. Cunningham, A. T. Blaker, and A. C. Coward, 2015: The North Atlantic subpolar circulation in an eddy-resolving global ocean model. *J. Mar. Syst.*, **142**, 126–143, doi:10.1016/j.jmarsys.2014.10.007.

McCarthy, G. D., and Coauthors, 2015: Measuring the Atlantic meridional overturning circulation at 26°N. *Prog. Oceanogr.*, **130**, 91–111, doi:10.1016/j.pocean.2014.10.006.

McDonagh, E., and Coauthors, 2015: Continuous estimate of Atlantic oceanic freshwater flux at 26.5°N. *J. Climate*, **28**, 8888–8906, doi:10.1175/JCLI-D-14-00519.1.

Meinen, C. S., M. O. Baringer, and R. F. Garcia, 2010: Florida Current transport variability: An analysis of annual and longer-period signals. *Deep-Sea Res. I*, **57**, 835–846, doi:10.1016/j.dsr.2010.04.001.

Mielke, C. L., 2015: The North Atlantic deep western boundary current: Seasonal cycle, decadal variability and relation to the Atlantic meridional overturning circulation. Ph.D. thesis, Institut für Meereskunde, Universität Hamburg, 121 pp.

Msadek, R., W. E. Johns, S. G. Yeager, G. Danabasoglu, T. L. Delworth, and A. Rosati, 2013: The Atlantic meridional heat transport at 26.5°N and its relationship with the MOC in the RAPID array and the GFDL and NCAR coupled models. *J. Climate*, **26**, 4335–4356, doi:10.1175/JCLI-D-12-00081.1.

——, and Coauthors, 2014: Predicting a decadal shift in North Atlantic climate variability using the GFDL forecast system. *J. Climate*, **27**, 6472–6496, doi:10.1175/JCLI-D-13-00476.1.

Nycander, J., J. Nilsson, K. Döös, and G. Broström, 2007: Thermodynamic analysis of ocean circulation. *J. Phys. Oceanogr.*, **37**, 2038–2052, doi:10.1175/JPO3113.1.

Rhines, P. B., S. Häkkinen, and S. A. Josey, 2008: Is oceanic heat transport significant in the climate system? *Arctic-Subarctic Ocean Fluxes: Defining the Role of the Northern Seas in Climate*, R. R. Dickson, J. Meincke, and P. B. Rhines, Eds., Springer, 87–109.

Roemmich, D., and C. Wunsch, 1985: Two transatlantic sections: Meridional circulation and heat flux in the subtropical North

Atlantic Ocean. *Deep-Sea Res. I*, **32**, 619–664, doi:10.1016/0198-0149(85)90070-6.

Rosmond, T., J. Teixeira, M. Peng, T. Hogan, and R. Pauley, 2002: Navy Operational Global Atmospheric Prediction System (NOGAPS): Forcing for ocean models. *Oceanography*, **15** (1), 99–108, doi:10.5670/oceanog.2002.40.

Sarafanov, A., and Coauthors, 2012: Mean full-depth summer circulation and transports at the northern periphery of the Atlantic Ocean in the 2000s. *J. Geophys. Res.*, **117**, C01014, doi:10.1029/2011JC007572.

Talley, L. D., 2003: Shallow, intermediate, and deep overturning components of the global heat budget. *J. Phys. Oceanogr.*, **33**, 530–560, doi:10.1175/1520-0485(2003)033<0530:SIADOC>2.0.CO;2.

——, 2008: Freshwater transport estimates and the global overturning circulation: Shallow, deep and throughflow components. *Prog. Oceanogr.*, **78**, 257–303, doi:10.1016/j.pocean.2008.05.001.

Uppala, S. M., and Coauthors, 2005: The ERA-40 Re-Analysis. *Quart. J. Roy. Meteor. Soc.*, **131**, 2961–3012, doi:10.1256/qj.04.176.

Wijffels, S. E., 2001: Ocean freshwater transport. *Ocean Circulation and Climate: Observing and Modelling the Global Ocean*, G. Siedler, J. Church, and J. Gould, Eds., International Geophysics Series, Vol. 77, Academic Press, 475–488.

Wunsch, C., 2005: The total meridional heat flux and its oceanic and atmospheric partition. *J. Climate*, **18**, 4374–4380, doi:10.1175/JCLI3539.1.

Xu, X., W. J. Schmitz Jr., H. E. Hurlburt, P. J. Hogan, and E. P. Chassignet, 2010: Transport of Nordic Seas overflow water into and within the Irminger Sea: An eddy-resolving simulation and observations. *J. Geophys. Res.*, **115**, C12048, doi:10.1029/2010JC006351.

——, ——, ——, and ——, 2012: Mean Atlantic meridional overturning circulation across 26.5°N from eddy-resolving simulations compared to observations. *J. Geophys. Res.*, **117**, C03042, doi:10.1029/2011JC007586.

——, H. E. Hurlburt, W. J. Schmitz Jr., R. J. Zantopp, J. Fischer, and P. J. Hogan, 2013: On the currents and transports connected with the Atlantic meridional overturning circulation in the subpolar North Atlantic. *J. Geophys. Res. Oceans*, **118**, 502–516, doi:10.1002/jgrc.20065.

——, E. P. Chassignet, W. E. Johns, W. J. Schmitz Jr., and E. J. Metzger, 2014: Intraseasonal to interannual variability of the Atlantic meridional overturning circulation from eddy-resolving simulations and observations. *J. Geophys. Res. Oceans*, **119**, 5140–5159, doi:10.1002/2014JC009994.

——, P. B. Rhines, E. P. Chassignet, and W. J. Schmitz Jr., 2015: Spreading of the Denmark Strait overflow water in the western subpolar North Atlantic: Insights from eddy-resolving simulations with a passive tracer. *J. Phys. Oceanogr.*, **45**, 2913–2932, doi:10.1175/JPO-D-14-0179.1.

Zika, J. D., M. H. England, and W. P. Sijp, 2012: The ocean circulation in thermohaline coordinates. *J. Phys. Oceanogr.*, **42**, 708–724, doi:10.1175/JPO-D-11-0139.1.

——, W. P. Sijp, and M. H. England, 2013: Vertical heat transport by ocean circulation and the role of mechanical and haline forcing. *J. Phys. Oceanogr.*, **43**, 2095–2112, doi:10.1175/JPO-D-12-0179.1.

Zweng, M. M., and Coauthors, 2013: *Salinity*. Vol. 2, *World Ocean Atlas 2013*, NOAA Atlas NESDIS 74, 39 pp.